Title: “Metformin Impairs Intestinal Fructose Metabolism”

Authors:
Wenxin Tong[1], Sarah A. Hannou[1,3], Ashot Sargsyan[1], Guo-Fang Zhang[1,2], Paul A. Grimsrud[1,2], Inna Astapova[1,2,3], and Mark A. Herman[1,2,3]

1 Duke Molecular Physiology Institute, Duke University, Durham, North Carolina, USA;
2 Division of Endocrinology, Metabolism, and Nutrition, Duke University, Durham, North Carolina, USA;
3 Division of Endocrinology, Diabetes, and Metabolism, Baylor College of Medicine, Houston, Texas, USA

Corresponding Author:
Mark A. Herman; Division of Endocrinology, Diabetes, and Metabolism, Baylor College of Medicine, Houston, Texas, USA
mark.herman@bcm.edu

Abstract

Objective: To investigate the effects of metformin on intestinal carbohydrate metabolism *in vivo*.

Method: Male mice preconditioned with a high-fat, high-sucrose diet were treated orally with metformin or a control solution for two weeks. Fructose metabolism, glucose production from fructose, and production of other fructose-derived metabolites were assessed using stably labeled fructose as a tracer.

Results: Metformin treatment decreased intestinal glucose levels and reduced incorporation of fructose-derived metabolites into glucose. This was associated with decreased intestinal fructose metabolism as indicated by decreased enterocyte F1P levels and diminished labeling of fructose-derived metabolites. Metformin also reduced fructose delivery to the liver. Proteomic analysis revealed that metformin coordinately down-regulated proteins involved carbohydrate metabolism including those involved in fructolysis and glucose production within intestinal tissue.

Conclusion: Metformin reduces intestinal fructose metabolism, and this is associated with broad-based changes in intestinal enzyme and protein levels involved in sugar metabolism indicating that metformin's effects on sugar metabolism are pleiotropic.

Key words

Metformin, glucose production, fructose metabolism, isotope-tracing metabolomics, proteomics

45 **Highlights**

46 - Metformin decreases intestinal fructose absorption, metabolism, and fructose
47 delivery to the liver.
48 - Metformin reduces intestinal glucose production from fructose-derived
49 metabolites.
50 - Metformin reduces protein levels of multiple metabolic enzymes involved in
51 fructose and glucose metabolism in intestinal tissue.

52

53 **Introduction**

54 Metformin is a first-line anti-diabetic drug and the most widely prescribed oral anti-
55 hyperglycemic worldwide [1]. Beneficial effects of metformin have also been suggested
56 for people with obesity [2], non-alcohol fatty liver disease [3], Alzheimer's disease [4], and
57 some cancers [5; 6]. Even though metformin has been investigated intensively for
58 decades, the target organ(s) and the underlying mechanism of metformin's beneficial
59 effects remain controversial.

60 Metformin's anti-diabetic effects are often attributed to its ability to reduce
61 endogenous glucose production [7; 8]. Because the liver is the major site of
62 gluconeogenesis in mammals, most studies have focused on metformin's effects on liver
63 tissue [9]. However, the role of liver in metformin's actions is receiving more scrutiny as
64 therapeutic doses of metformin may not produce sufficient concentrations of metformin in
65 hepatocytes to mediate its observed systemic effects [8; 10]. In contrast with liver,
66 metformin is highly concentrated in intestinal tissue [11; 12]. In intestinal tissue, metformin
67 may achieve concentrations that are 100 to 300-fold higher than circulating plasma levels,
68 and ~ 2-10-fold higher than that in the liver [11; 12]. This suggests that metformin has the
69 potential to have outsized impact on intestinal function to regulate systemic glucose
70 homeostasis [13]. Metformin may regulate glycemia through effects on the intestine via
71 multiple mechanisms. For instance, a recent study showed that metformin's glucose-
72 lowering effect is mediated through activating the PEN2-directed lysosomal AMPK
73 pathway in intestinal tissue and not in liver [14]. Additionally, multiple studies in both
74 humans and preclinical models using a F18- fluorodeoxyglucose (F18-FDG) tracer
75 indicate that metformin enhances glucose uptake in the colon and possibly the small
76 intestine [13; 15; 16]. Recent studies from our group and others demonstrated that
77 fructose is metabolized at high rates in intestinal tissue and contributes to intestinal
78 glucose production [17; 18]. In this study, using fructose to assess enterocyte metabolic
79 function and as a gluconeogenic tracer, we show that short-term treatment of mice with
80 metformin impairs intestinal carbohydrate metabolism and reduces intestinal glucose
81 production adding to the mechanisms by which metformin impacts systemic glucose
82 homeostasis.

83

Methods

Materials:

Metformin (hydrochloride) was purchased from Cayman Chemical (No. 13118). D-Fructose was purchased from VWR international (VWRV0226). [U-^{13}C]-fructose, and [U-^{13}C]-fructose-6-phosphate (M6-F6P) were purchased from Cambridge Isotope Labs (CLM-1553-PK, and CLM-8616 respectively). Norvaline and D-[1,6-$^{13}C_2$]-fructose (M2-fructose) were purchased from Sigma-Aldrich (53721 and 587613 respectively).

Animals:

All animal experiments were approved by Duke Institutional Animal Care and Use Committee. 17-18 weeks old wild-type C57/BL6J (Stock# 000664) male mice were purchased from The Jackson Laboratory and maintained in a pathogen free vivarium at Duke University. All animals were maintained at ~ 22°C on a 12-hour light-dark cycle (6 AM to 6 PM) and adapted for at least one week before any experimental procedure or intervention. Within experiments, mice were divided randomly into either water control or metformin treatment groups. To prepare the metformin oral-gavage solution, 500 mg metformin was dissolved in 20 mL sterile water and aliquoted into 14 vials stored at 4 °C. After pretreatment of all mice with 1 week of high-fat, high-sucrose diet (45% fat, 20% sucrose, Research Diet, D12451i), we randomly distributed mice to two groups and orally gavaged water or metformin solutions at a dose of 10 μL/g body weight. After two weeks of metformin or water administration, an i.p. glucose tolerance test (GTT) was conducted. Two days after the i.p. GTT was performed, mice were sacrificed 30 minutes after fructose gavage (1:1 mixture of unlabeled fructose and [U-^{13}C]-fructose). Unless otherwise noted, all procedures including oral gavage and body weight measurement were performed at 9:30 AM. Euthanasia after fructose gavage was performed at 2 PM, 5 hours after food removal at 9 AM.

Glucose tolerance test:

Animals were fasted for 5 hours starting at 9 AM. At 2PM, animal body weight was measured, and sterile glucose solution was injected intraperitoneally at a dose of 1.5 g/Kg

114 body weight. Glycemia was measured using a drop of blood drawn from a nicked tail vein
115 via glucometer (Bayer Contour) at 0, 15, 30, 60, 90, and 120 minutes after injection.
116
117 Animal euthanasia and sample/tissue harvest:
118 Animals were euthanized under isoflurane anesthesia 30 minutes after fructose
119 gavage (1:1 mixture of unlabeled fructose and [U-^{13}C]-fructose at 4g/Kg body weight).
120 Mice were anesthetized under continuous oxygen following the guidelines recommended
121 by the Duke Institutional Animal Care and Use Committee. Once deep anesthesia was
122 confirmed by a toe pinch, blood samples from the tail vein were harvested. Laparotomy
123 was subsequently performed, and the portal vein was exposed. Clean scissors were used
124 to make a small incision in the portal vein, and blood (200 μL) was extracted using a 1
125 mL syringe from the peritoneal cavity and transferred to an EDTA-coated blood collection
126 tube (Sarstedt, 16.440.100). The liver and intestine were removed from the abdominal
127 cavity. Liver tissue was snap frozen in liquid nitrogen. The small intestine extending from
128 0.5 cm distal to the end of the stomach and extending to 0.5 cm proximal to the cecum
129 was excised, flushed with ice-cold PBS and snap frozen in liquid nitrogen.
130
131 Gas chromatography-mass spectrometry (GC/MS):
132 Plasma was prepared from collected blood by centrifugation at 2,000 g, 4°C for 15
133 minutes. Tissue samples were powdered under liquid N_2. 0.2 mM 2-Deoxy-D-glucose
134 (2DG), 0.2 mM M2-fructose, 0.1 nM M6-F6P or 0.1 mmol norvaline was added to 10 μL
135 plasma samples or 10 mg powdered tissue samples as an internal standard for the
136 measurement of glucose, fructose or TCA cycle intermediates respectively. After that,
137 400 μL MeOH, 400 μL ddH2O, and 400 μL chloroform were added sequentially and briefly
138 vortexed after each addition. After centrifugation at 12,000 g for 15 minutes, supernatants
139 were collected and dried under nitrogen.
140 Relative quantification and enrichment measurements for glucose, glycerate, F1P,
141 and GA3P: Dried sample residues were derivatized with methoxylamine hydrochloride
142 and trimethylsilyl (TMS) sequentially. Specifically, 25 μL of methoxylamine hydrochloride
143 (2% (w/v) in pyridine) was added to the dried residues and incubated for 90 minutes at
144 40°C before the addition of 35 μL of TMS and incubation for 30 minutes at 60°C. The

145 samples were then centrifuged for 2 minutes at 12,000 g and the supernatants of
146 derivatized samples were transferred to GC vials for further analysis.
147 Absolute quantification of fructose: the dried residues were derivatized with
148 methoxylamine hydrochloride and propionic anhydride sequentially adapted from a
149 previously described method [19]. 25 µL of methoxylamine hydrochloride (2% (w/v) in
150 pyridine) was added to the dried residues and incubated for 60 minutes at 70°C. After
151 centrifugation for 2 minutes at 12,000 g, 50 µL propionic anhydride was added and
152 incubated for 30 minutes at 60°C prior to another round of drying under nitrogen. The
153 dried residues were resuspended with 55 µl pure ethyl acetate and transferred to GC vials
154 for analysis.
155 Relative quantification and enrichment measurements of TCA cycle intermediates:
156 Dried residues were derivatized with methoxylamine hydrochloride and
157 tertbutyldimetheylchloros (TBDMS) sequentially as previously described [3]. 25 µL of
158 methoxylamine hydrochloride (2% (w/v) in pyridine) was added to the dried residues and
159 incubated for 90 minutes at 40°C before the addition of 35 µL of TBDMS and incubation
160 for 30 minutes at 60°C. The samples were then centrifuged for 2 minutes at 12,000 g and
161 the supernatants of derivatized samples were transferred to GC vials for further analysis.
162 GC/MS analysis was conducted using an Agilent 7890B GC system and Agilent
163 5977A Mass Spectrometer. 1 µL of the derivatized sample was injected into the GC
164 column. The GC temperature gradient started at 90°C, increased to 260°C at the speed
165 of 9°C per minute and further increased to 290 °C at the speed of 30°C per minute. Then
166 the temperature was held at 290°C for 5 minutes with a run time of 24.9 minutes.
167 Ionization was conducted by EI at 70 eV with Helium flow at 1 mL/min. Temperatures of
168 the source, the MS quad, the interface, and the inlet were maintained at 230°C, 150°C,
169 280°C, and 250°C, respectively. Mass spectra were recorded in mass scan mode from
170 m/z 50 to 700. The levels of metabolites were calculated based on the area of the peak
171 at its specified retention time. Total ion counts (A.U.) of metabolites were assessed as
172 the sum of its isotopologues and normalized to their specific standards as detailed above
173 and below.
174
175 Stable Isotope Analysis and Average Carbon-13 Label Incorporation Rates:

176 Isotopologues containing 0, 1, to n heavy atom(s) in a molecule were referred as
177 M+0, M+1, to M+n respectively. The retention times of individual metabolites and their
178 isotopomers are described in Supplementary Table 1. Isotope enrichment and labeling
179 analysis in this study were corrected for natural isotope distribution as previously
180 described [20; 21]. Specifically, the stable isotope enrichment of each metabolite in
181 plasma and tissue samples was corrected based on the natural isotope distribution
182 measured in the same type of sample treated without labeled molecules. For example,
183 the natural isotope distribution matrix of individually measured metabolites in the blood
184 samples were experimentally determined by assaying and averaging the blood samples
185 from animals who had not received any treatment with isotopically labeled sources.
186 The average carbon-13 incorporation was calculated according to the equation as
187 previously described in reference (18). Specifically, n_{M+i} refers to the number of ^{13}C
188 carbons in the isotopomer (M+i). For example, n = 0 for M+0, n = 1 for M+1, and n = 2 for
189 M+2, and so on. "A" refers to the corresponding percentage abundance of the isotopomer.
190 N refers to the total carbon number, which for glucose, N = 6.
191

192 $$Average\ C13\ incorporation = \frac{(\sum_{i=0}^{N} n_{M+i}\ * A)}{N}$$

193

194 Quantification of metabolites:
195 The relative quantification of total glucose, F1P, and GA3P levels were calculated
196 as the ratio derived from the sum of total ion counts of all isotopologues to their specific
197 internal standards (2DG for glucose and M6-F6P for F1P and GA3P respectively). The
198 absolute quantification of M+0 and M+6 fructose isotopologues were calculated as the
199 ratio of M+0 fructose ion counts or M+6 fructose ion counts to M+2 fructose ion counts
200 which is derived from the M2-fructose internal standard respectively.
201 For the quantification of glucose derived from any fructose carbons, we first
202 calculated the stable isotope enrichment of each isotopologue of glucose after correction
203 for the natural isotope distribution. Because fructose was administered as an equal
204 mixture of unlabeled and [U-^{13}C]-labeled fructose, levels of glucose derived from any
205 fructose carbons were calculated as twice the total glucose ion counts multiplied by the

206 corrected percentage of the sum of glucose isotopomers containing any ^{13}C. Levels of
207 glucose with three fructose-derived carbons were calculated as twice the total glucose
208 ion counts multiplied by the corrected percentage of M+3 glucose isotopomers.
209
210 Proteomics Sample Preparation:
211 Samples from mice treated with and without metformin (n=5) underwent large-
212 scale analysis of relative protein abundance changes as described previously [22]. For
213 each sample, approximately 15 mg of pulverized mouse intestinal tissue was solubilized
214 in ice-cold urea Lysis buffer (8 M urea in 50 mM Tris, pH 8.0, 40 mM NaCl, 2 mM $MgCl_2$,
215 1x Roche cOmplete ULTRA EDTA-free protease inhibitor mini tablet, 1x PhosStop
216 phosphatase inhibitor tablet, 5 mM NaF and 10 mM Na pyrophosphate). Samples were
217 lysed with a combination of disruption with a TissueLyzer (Qiagen) for 30 sec at 30 Hz,
218 subjected to three freeze-thaw cycles, and sonication with a probe sonicator. After
219 centrifugation at 10,000 g for 10 min at 4°C, protein concentration in the supernatant was
220 determined by BCA, and a 400 µg aliquot of each was adjusted to 2 mg/mL with Urea
221 Lysis Buffer. To reduce and alkylate cysteine residues, samples were incubated with 5
222 mM DTT at 32 °C for 30 min, cooled to RT, and incubated with 15 mM iodoacetamide for
223 30 min in the dark at RT. Following quenching of unreacted iodoacetamide by the addition
224 of equimolar DTT (up to 15 mM), samples were enzymatically digested with LysC (100:1
225 w/w, protein to enzyme) at 32 °C for 4 hr. After dilution to 1.5 M urea with 50 mM Tris (pH
226 8.0), 5 mM $CaCl_2$, samples were digested with trypsin (50:1 w/w, protein:enzyme)
227 overnight at 32 °C. Samples were acidified to 0.5% TFA and centrifuged at 10,000 ×g for
228 10 min at RT to pellet insoluble material. Supernatant containing soluble peptides was
229 subjected to solid phase extraction (SPE) with a Waters 50 mg tC18 SEP-PAK column to
230 remove salt, eluting once with 500 µL 25% acetonitrile/0.1% TFA and twice with 500 µL
231 50% acetonitrile/0.1% TFA. The eluate was frozen and dried by speed vac. Samples were
232 resuspended in 100 µL of 200 mM triethylammonium bicarbonate (TEAB), vortexed,
233 mixed with a different 10-plex Tandem Mass Tag (TMT) reagent (0.8 mg resuspended in
234 50 µL 100% acetonitrile), shaken for 4 hr at RT, and quenched with 0.8 µL 50%
235 hydroxylamine (shaking for 15 min at RT). All samples were mixed, frozen, and dried by
236 speed vac. The mixture was resuspended in 1 mL 0.5% TFA and subjected to SPE again

237 with a Waters 100 mg tC18 SEP-PAK SPE column as described above and the eluate
238 was frozen and dried by speed vac. The 4 mg TMT-labeled peptide mixture was
239 fractionated by high pH reversed-phase (HPRP) chromatography. After each of 12
240 fractions was lyophilized and resuspended in 1 mL 80% acetonitrile/0.15% TFA, 50 µL
241 was removed for analysis of unmodified peptides, frozen, and dried by speed vac.
242
243 Proteomics data acquisition:
244 Samples were analyzed by nanoflow liquid chromatography (nLC) on an EASY-nLC 1200
245 UH-PLC, followed by electrospray ionization (ESI) with an EASY-Spray source, and
246 tandem mass spectrometry (MS/MS) with a Q Exactive Plus Hybrid Quadrupole-Orbitrap
247 (Thermo Fisher Scientific). Sample fractions were resuspended in 22 µL of 0.1% FA and
248 were analyzed with triplicate runs, injecting 1 µL for the first and adjusting the volume for
249 subsequent runs to target an MS1 base peak intensity of 1×10^{10}. For each injection, the
250 sample was first trapped on an Acclaim PepMap 100 C18 trapping column (3 µg particle
251 size, 75 µm ×20 mm) with solvent A (0.1% FA) at a variable flow rate dictated by a
252 maximum pressure of 500 bar, after which the analytical separation was performed over
253 a 140 min gradient (flow rate of 300 nL/min) of 2% to 40% solvent B (90% ACN, 0.1%
254 FA) using an Acclaim Pep-Map RSLC C18 analytical column (2 µg particle size, 75µg
255 ×500 mm column (Thermo Fisher Scientific) with a column temperature of 55 °C. MS1
256 (precursor ions) was performed at 70,000 resolution with an AGC target of 3×10^{6} ions
257 and a maximum injection time (IT) of 60 ms. MS2 spectra (product ions) were collected
258 by data-dependent acquisition of the top 10 most abundant precursor ions with a charge
259 greater than 1 per MS1 scan, with dynamic exclusion enabled for a window of 30 s.
260 Precursor ions were filtered with a 0.7 m/z isolation window and fragmented with a
261 normalized collision energy of 30. MS2 scans were performed at 35,000 resolution, with
262 an AGC target of 1×10^{5} ions and a maximum IT of 60 ms. All raw files were uploaded to
263 Proteome Xchange (PXD041833) and jPOST (JPST002144) [23; 24]
264
265 Proteomics data analysis:
266 Raw files were processed with Proteome Discoverer 2.5 (PD2.5) from Thermo Fisher
267 Scientific. A complete mouse proteome FASTA file containing 55,315 reviewed (Swiss-

268 Prot) and unreviewed (TrEMBL) protein sequences, downloaded from UniProt on
269 8/15/2022, was imported into PD2.5. “Treatment” (metformin) versus “Water” (control)
270 were incorporated as “Study Factors”. MS1 precursor mass recalibration was performed
271 after a pre-search using the Spectrum Files RC node. Subsequent searches with Sequest
272 HT were conducted at 10 ppm (recalibrated) and 0.02 Da mass tolerances for precursor
273 and fragment ions, respectively. Modifications considered included oxidation on
274 methionine (variable + 15.995 Da), carbamidomethylation of cysteine (fixed + 57.021 Da),
275 and TMT6plex addition to lysine peptide N-termini (fixed + 229.163 Da). Searches allowed
276 for up to 2 missed K/R cleavages by trypsin (full specificity). Percolator [9] was used to
277 filter peptide spectral matches (PSMs) to an estimated FDR of less than 1%. The Peptide
278 Isoform Grouper node was used to collapse PSMs down to unique peptides, while
279 maintaining FDR < 1% at the peptide level. The Protein FDR Validator node was used to
280 group peptides into proteins using the rules of strict parsimony and maintain FDR < 1%
281 at the protein level. The Reporter Ion Quantifier node was used to filter PSMs for
282 quantitative quality, setting an upper threshold 50% precursor co-isolation and an average
283 reporter ion S/N> 2.5. For PSMs meeting these criteria, quantitative values were summed
284 together at the peptide and protein levels (after adjusting for TMT isotope impurities).
285 Unique peptides and Razor peptides were used for protein quantitation calculations,
286 excluding peptides with oxidized methionine. Quantitative values were normalized for any
287 deviations from equal total peptide signal on each TMT “channel”. Data were further
288 analyzed in R. PCA analysis was performed within each conditions, water and metformin
289 specifically, for outlier detection. One sample in each group appeared to be an extreme
290 outlier compared to the other samples in the group and were not used in subsequent
291 analysis. Data analysis was conducted in R 4.0. Differential expression analysis was
292 conducted with the Limma and DEseq2 packages [25; 26]. Data were visualized with the
293 ggplot2 package and hierarchical clustering heatmaps were generated using the
294 pheatmap package where Pearson correlation was used as the distance measure.
295
296 Western Blot:
297 20 to 30 mg intestinal tissue samples were homogenized in 0.5 mL cell signaling lysis
298 buffer that contains 20 mM Tris-HCl, 150 mM NaCl, 1 mM Na2EDTA, 1 mM EGTA, 1%

299 Triton and further supplemented with protease inhibitors (Sigma-Aldrich, P8340) and
300 phosphatase inhibitor cocktail (Pierce, A32957). After centrifugation at 12,000 g for 15
301 minutes, the supernatant was transferred to a fresh tube to measure protein concentration
302 using the BCA method (ThermoFisher, 23225). Approximately 35 ug of protein was
303 loaded per lane for SDS-PAGE electrophoresis. After electrophoresis, immunoproteins
304 were transferred to PVDF membranes. The membranes were then incubated with primary
305 antibodies overnight at 4 °C with gentle rocking after blocking with 5% solution of BSA
306 (Cytivia, SH30574.02) at room temperature for 1 hour. Primary antibodies used in this
307 work are as follows: anti-AMPK (Cell Signaling, 5831S), anti-AMPK (phospho T172)
308 antibody (Cell Signaling, 2635S), and anti-P85 (Upstate, 06-496). Blots were incubated
309 with appropriate secondary antibody after washing with TBST for 3 times.
310 Chemiluminescence was conducted using the Clarity Western ECL substrate kit (Bio-
311 Rad, 1705061) and membranes were imaged on ChemiDoc XP (Bio-Rad). Quantification
312 of blots was conducted using ChemiDoc XP associated Image Lab software v6.0. For
313 loading normalization, whole lane proteins were quantified using Bio-Rad Stain free
314 technology.
315
316 Statistics:
317 All data are presented as mean ± SEM. Comparison of metabolite levels between
318 the metformin group and controls were conducted using a two-tailed student's t-test in
319 GraphPad Prism. Statistical significance was assumed at p less than 0.05.
320
321 **Results**
322 **Short-term metformin treatment improves glucose tolerance without altering**
323 **fasting glycemia**
324 To investigate metformin's role in intestinal metabolism, 18-week-old wildtype
325 C57BL/6J mice were preconditioned with 1 week of high-fat, high-sucrose diet (45% Fat,
326 40% Sucrose) and then orally gavaged with metformin at a daily dose of 250 mg/kg of
327 body weight for two weeks. This dose of metformin in mice is reported to achieve
328 circulating concentrations of ~ 5 - 10 μM which is comparable to that in humans with Type-
329 2 Diabetes (T2D) taking 1 - 2 g metformin per day [27].

330 Metformin treatment did not affect body weight (Figure 1A, metformin: 33.5 ± 2.7
331 vs water: 34.2 ± 2.1 g). This is similar to observations that short-term metformin treatment
332 does not significantly impact body weight in human patients [28]. Fasting glycemia
333 remained similar between the metformin and control groups (Figure 1B). Whereas
334 metformin had no significant effect on body weight or fasting glycemia, 2 weeks of
335 metformin enhanced glucose tolerance (Figure 1C and D) with a reduction in glycemia at
336 the 30-minute time point (metformin: 292.44 ± 92.57 mg/dL vs water: 393.89 ± 87.23
337 mg/dL, $p<0.05$) and decreased area under the curve (metformin: 27790 ± 3326 A.U. vs
338 water: 34600 ± 2676 A.U., $p<0.05$). Thus, short-term metformin treatment enhanced
339 glucose tolerance without significant changes in body weight.
340

341 **Short-term metformin treatment decreases intestinal fructose metabolism and**
342 **fructose delivery to the liver**

343 The intestine is capable of robust fructose metabolism and a large portion of
344 intestinally metabolized fructose is used to produce glucose within intestinal tissue (Figure
345 2A) [17; 18]. After transport into the cell, fructose is first metabolized to fructose-1-
346 phosphate (F1P) followed by further metabolism to dihydroxyacetone phosphate (DHAP)
347 and glyceraldehyde (GA). Glyceraldehyde can be converted into glyceraldehyde-3-
348 phosphate (GA3P) via triokinase or into glycerate via aldehyde dehydrogenase. Glycerate
349 production tends to increase following a bolus of fructose and saturation of triokinase [29].
350 Fructose-derived triose phosphates then enter the glycolytic/gluconeogenic triose-
351 phosphate pool and can be used either for glucose production or can be further
352 metabolized to pyruvate/lactate and potentially enter the TCA cycle for oxidation. We
353 used ^{13}C-labeled fructose as a tracer to investigate the effects of metformin on intestinal
354 fructose and carbohydrate metabolism including glucose production. After a 5 hour fast,
355 we gavaged animals from both metformin and control groups with a 1:1 mixture of
356 unlabeled fructose and fructose that was universally labeled with carbon-13 ([U-^{13}C]-
357 fructose).

358 The levels of F1P were markedly reduced (from 14.20 ± 3.85 to 6.50 ± 3.54 A.U.,
359 $p<0.01$) in the intestinal tissue of animals treated with metformin versus water (Figure
360 2B). Metformin treatment reduced the enrichment of isotope-labeled three-carbon

361 metabolites, glyceraldehyde 3-phosphate (GA3P) and glycerate in intestinal tissue
362 (Figure 2C and D). These data indicate that fructose catabolism in intestinal tissue is
363 impaired by metformin treatment. Reductions in intestinal fructose metabolism could lead
364 to increased hepatic fructose delivery and contribute to fructose-induced metabolic
365 disease [30]. However, we observed that metformin treatment decreased portal vein M+0
366 and M+6 fructose levels by ~ 34% (Figure 2E). Reduced intestinal fructose metabolism
367 in combination with decreased portal fructose levels indicates that metformin impairs
368 intestinal fructose absorption. Additionally, the reduction in portal fructose following
369 metformin treatment indicates that metformin may reduce fructose delivery to the liver.
370 Consistent with this, metformin reduced levels of hepatic F1P (3.14 ± 1.59 to 1.25 ± 0.68
371 A.U., $p<0.05$, Figure 2F). Metformin treatment produced similar reductions in hepatic
372 GA3P levels (0.19 ± 0.10 to 0.08 ± 0.03 A.U., $p<0.05$, Figure 2G). Altogether, these results
373 indicate that two weeks of metformin treatment is sufficient to decrease intestinal fructose
374 metabolism and reduce fructose delivery to the liver.
375
376 **Short-term metformin treatment blunts intestinal glucose production**
377 At euthanasia—30 minutes after fructose gavage—metformin reduced glucose
378 levels within intestinal tissue by 47% compared to control (Figure 3A). The reduced
379 glucose levels within intestinal tissue could be caused either by an increase in intestinal
380 glucose metabolism as suggested by experiments using FDG-glucose as a tracer [13],
381 reduced intestinal glucose production, or a combination of the two. Within intestinal tissue,
382 metformin also reduced the percentage of glucose containing fructose derived labeled
383 carbons (Figure 3B). At this time point, glycemia in systemic circulation is only reduced
384 by 13% in metformin treated mice compared to controls (Figure 3C). The labeling of
385 intestinal glucose with fructose-derived, labeled carbons is ~ 2-fold higher than in
386 peripheral circulation (Figure 3B and 3D). In combination, these results show that glucose
387 derived from fructose is being produced locally within the intestinal tissue. Glucose
388 produced from fructose within enterocytes is generated following metabolism of fructose
389 to trioses and will therefore predominately contain three fructose-derived carbons (Figure
390 2A and 3B). Within intestinal tissue, metformin reduced the labeling of glucose compared
391 to controls (Figure 3B) and reduced the levels of glucose containing any or three fructose-

392 derived carbons (Figure 3E and F) to a larger extent than glucose without fructose derived
393 carbons (Figure 3G). The reduction in intestinal glucose containing fructose-derived
394 carbons accounts for most of the reduction in intestinal glucose levels in the metformin
395 treated mice (comparing Fig 3A and 3E). Thus, the reduction in intestinal glucose
396 production from fructose is a major contributor to reduced intestinal glucose levels
397 following metformin treatment. This is consistent with metformin's effect to reduce
398 fructose absorption and metabolism as indicated in Figure 2.
399

400 **Short-term metformin treatment decreases fructose incorporation into the TCA**
401 **cycle.**

402 We previously demonstrated that fructose gavage rapidly labels the intestinal TCA
403 cycle pool which is a major contributor to circulating TCA cycle metabolites [31]. We next
404 investigated whether metformin also affects this process. The enrichment of labeled TCA
405 cycle intermediates was reduced in intestinal tissue of metformin treated mice (Figure 4A-
406 C). Metformin treatment produced a similar reduction in portal plasma TCA cycle
407 metabolite enrichment (Figure 4D-F). These data support our previous finding that the
408 intestine is a major source of circulating TCA cycle intermediates. Moreover, these results
409 indicate that labeling of circulating TCA cycle metabolites is responsive to metformin
410 treatment and measurement of this labeling pattern in blood may be a useful surrogate
411 index of intestinal metabolic function.

412 Whereas metformin uniformly reduced TCA cycle enrichment in both intestinal
413 tissue and portal blood samples, its effect on TCA cycle metabolite levels was mixed.
414 Metformin reduced citrate levels in both intestinal tissue and portal circulation (Figure 4G
415 and H). In contrast, metformin produced no changes in either tissue or circulating
416 succinate and produced an isolated increase in portal malate levels without a change in
417 malate in intestinal tissue although the variance was high for malate measurements in
418 tissue. The changes in TCA cycle metabolite levels may suggest that metformin inhibits
419 malate to citrate conversion in the TCA cycle, potentially via inhibition of malate
420 dehydrogenase. This would be consistent with metformin's purported effects to inhibit
421 Complex I activity as malate dehydrogenase donates electrons to Complex I and its
422 activity is closely coupled to that of the electron transport chain [32-35].

423

424 **Metformin reduces the abundance of intestinal proteins involved in carbohydrate**
425 **metabolism.**

426 As isotope-tracing metabolomics indicated that metformin reduced intestinal
427 fructose catabolism and glucose production, we next aimed to investigate molecular
428 mechanisms contributing to these changes via proteomics in intestinal tissue. In total,
429 5,328 proteins were quantified and annotated via our discovery proteomics
430 (Supplementary Table 2). Principal component analysis (PCA) using all quantified
431 proteins identified two clusters that separate the treatment groups (Figure 5A). However,
432 the 95% confidence intervals for the metformin and control clusters overlap suggesting
433 that global protein expression levels within the intestine were not markedly different
434 between treatment conditions (Figure 5A).

435 A total of 1,942 proteins were identified as differentially abundant between
436 metformin and control groups at $p < 0.05$ (two-tailed student's t-test). After adjusting for
437 repeated measures by the Benjamini and Hochberg method, a total of 219 proteins were
438 identified as differentially abundant at $P_{adjusted} < 0.05$ and $|\log_2 \text{fold-change}| > 0.5$ (Figure
439 5B and Supplementary Table 3). Many of the top-ranked differentially abundant proteins
440 are associated with metabolic process including gluconeogenic enzymes such as Fbp1
441 and G6pc (Figure 5B). Despite variability in protein abundance levels within groups,
442 unsupervised K-means clustering segregated metformin treated from untreated mice
443 (Figure 5C). Pathway analysis using differentially expressed proteins with $P_{adjusted} < 0.05$
444 suggested that metformin treatment affected multiple metabolic pathways in the intestinal
445 tissue (Supplementary Table 4 and 5). One of the top down-regulated pathways in
446 intestinal tissue from the metformin group is "Glycolysis and Gluconeogenesis (WP157)"
447 (Figure 5D). Other metabolic pathways demonstrating downregulation with metformin
448 treatment include the "Electron Transport Chain (WP295)" and "Oxidative
449 Phosphorylation", pathways potentially complementary to the putative effects of
450 metformin to inhibit mitochondrial function [36; 37] (Figure 5D). In addition, proteins
451 associated with both glycolysis and gluconeogenic pathways, including pyruvate
452 carboxykinase (Pck1), Fructose 1,6-bisphosphatase (Fbp1), glucose 6-phosphatase
453 (G6pc1), lactate dehydrogenase (Ldhb), pyruvate dehydrogenase (Pdh1), malate

454 dehydrogenase (Mdh2), enolase 1 (Eno1), hexokinase (Hk1), pyruvate kinase (Pkm),
455 bisphosphoglycerate mutase (Bpgm), were markedly down-regulated in the metformin
456 group compared to controls (Figure 5E). Similarly, hexose transporters capable of
457 fructose transport including both GLUT5 (Slc2a5) and GLUT2 (Slc2a2), as well as key
458 fructolytic enzymes ketohexokinase (Khk) and aldolase, fructose-bisphosphate B (Aldob)
459 were all significantly down-regulated in metformin treated intestinal tissues (Figure 5F).
460 The reduction in glycolytic, gluconeogenic, and fructolytic transporters and enzymes are
461 consistent with the results from the metabolomic tracer studies that indicate that
462 metformin impairs intestinal fructose absorption and catabolism as well as glucose
463 production.
464

465 **Activation of AMPK signaling is likely to impact metformin's effects on intestinal**
466 **metabolic functions**

467 The proteomics study suggests that mitochondria, and especially the electron
468 transport chain, are impacted by metformin treatment through coordinate downregulation
469 of many of its constituent proteins (Figure 5D, Figure 6A, and Supplementary Table 4).
470 The ability of metformin to impact mitochondrial function is well documented [36-39].
471 Activation of AMPK is purported to play a central role in metformin's mechanism of action
472 and activation of AMPK may be mediated via metformin's ability to inhibit mitochondrial
473 Complex I and via other mechanisms [36; 40; 41]. We examined the abundance levels of
474 detectable proteins quantified in our proteomics data that are annotated within the "AMPK
475 signaling pathway (KEGG: mmu04152)" and conducted a PCA analysis using these 50
476 proteins. As is indicated in Figure 6B, abundance of components of the AMPK signaling
477 pathway in the intestine samples from metformin versus control treated mice tend to
478 segregate based on the first and second principal components (PC1 and PC2,
479 Supplementary Table 5). Our intestinal proteomics study only detected the α (Prkaa1,
480 Prkaa2) and γ subunits (Prkag1) of AMPK component (Figure 6C). Among these, the
481 abundance of Prkaa1 significantly decreased after metformin treatment while Prkaa2
482 tended to increase (Figure 6C). To further examine the role of AMPK signaling, we
483 measured the total protein levels of AMPKα and the phosphorylation of AMPKα at the Thr
484 172 site, a marker of AMPK activation. As expected, metformin treatment increased the

485 phosphorylation level of AMPKα Thr172 indicating that short-term metformin treatment
486 activates intestinal AMPK signaling (Figure 6D and E).
487
488 **Discussion**
489 Metformin is a widely prescribed anti-diabetic drug with uncertain target tissues
490 and mechanism of action. Identification of metformin's target tissue will facilitate the
491 understanding of metformin's glucose lowering effects and may promote the development
492 of additional therapies for metabolic diseases. Previous studies suggested the potential
493 of the intestine as an important metformin target since metformin concentrates to high
494 levels in intestinal tissue [11; 12]. Intravenous administration of metformin or reducing
495 intestinal metformin absorption impairs metformin's effects to lower glucose production
496 [42; 43]. Few studies have investigated the role of metformin on intestinal function and its
497 association with systemic glucose homeostasis. Among the studies focusing on the
498 intestine, the beneficial effects of metformin were suggested to closely associated with its
499 role on stimulating intestinal secretion of GLP-1 and GDF15 which are known to regulate
500 systemic glucose homeostasis [27; 37; 44]. To our knowledge, no study has directly
501 assessed metformin's effects on intestinal metabolic function using stable isotopic
502 tracers. In this study, we assessed intestinal fructose metabolism after an oral fructose
503 bolus (1:1 ratio of unlabeled:^{13}C-labeled fructose) to probe intestinal carbohydrate
504 metabolism after short-term metformin treatment. This methodology is based on recent
505 findings from our lab and others that fructose is rapidly metabolized in the small intestine
506 and can be readily used by the intestine to produce glucose [17; 18].
507 In this study, we observed that 30 minutes after fructose gavage, the majority of
508 glucose within intestinal tissue contained fructose-derived carbons and half contained
509 three fructose-derived carbons (Figure 3A, E, and F) in both metformin treated mice and
510 controls. In systemic circulation, enrichment of glucose with fructose-derived carbon was
511 ~ 50% lower than in intestinal tissue (Figure 3B vs 3D) indicative of dilution of intestinally
512 derived glucose in systemic circulation. This supports prior work indicating that fructose
513 is readily used as metabolic substrate for glucose production in the intestine and this
514 contributes significantly to whole-body glucose production [17; 18]. Our data

515 demonstrates that short-term metformin treatment reduced intestinal glucose production
516 from fructose and fructose delivery to the liver (Figure 2 and 3).
517 Metformin reduced intestinal glucose production, and this is associated with
518 enhanced glucose tolerance (Figure 1C and D). Importantly, these beneficial effects
519 occurred prior to significant weight changes (Figure 1A). Whether the effect of metformin
520 to reduce intestinal glucose production is a major mechanism by which metformin
521 enhances systemic glucose tolerance remains to be defined.
522 With the prevalence of high fructose corn syrup in the typical Western diet, the
523 potential for fructose consumption as a contributor to metabolic disease has attracted
524 increasing attention [45]. Studies conducted in both human and rodents support the
525 hypothesis that excessive fructose consumption can contribute to metabolic disorders
526 including obesity, insulin resistance, and NAFLD [46-48]. Intestinal tissue is a major site
527 of fructose metabolism and shields the liver from fructose induced metabolic disease [17],
528 as hepatic fructose metabolism is essential for the development of fructose related
529 pathologies like increased de novo lipogenesis, steatosis, and insulin resistance [30]. A
530 prior study suggested that fructose-induced metabolic disease may be attenuated by
531 metformin treatment in mice although this was attributed to an effect of metformin to alter
532 the microbiome and protect against deterioration of gut barrier function [49]. Our results
533 are consistent with a protective effect of metformin against fructose-induced metabolic
534 disease as we demonstrated that metformin decreased fructose delivery to the liver
535 (Figure 2E-G). These results might point towards a particularly beneficial effect of
536 metformin in people with diabetes and metabolic disease that consume excessive
537 amounts of dietary sugar.
538 In addition to decreasing fructose delivery to the liver, we also demonstrated that
539 metformin decreased intestinal fructose metabolism. Specifically, intestinal F1P levels
540 were nearly halved in the intestinal tissue of metformin treated animals when compared
541 to controls (Figure 2B). Additionally, significantly lower enrichment of isotope labeling was
542 detected in the downstream three-carbon phosphates and TCA cycle metabolites (Figure
543 2C and D, Figure 4 A-C). It is interesting that metformin treatment not only decreased
544 intestinal fructose metabolism, but also reduced the amount of fructose delivered to the
545 liver, suggesting the possibility that metformin treatment reduced intestinal fructose

546 absorption. Indeed, unbiased proteomics indicated that the abundance of luminal fructose
547 transporter GLUT5 and the basolateral glucose/fructose transporter GLUT2 were both
548 reduced by metformin treatment (Figure 5F). This finding seems contradictory to a recent
549 study where metformin increased GLUT2 expression in the colon and to a lesser extent
550 in the ileum [13]. This discrepancy may be due in part to differences in intestinal segments
551 analyzed between the two studies. Further investigation will be required to determine the
552 impact of metformin on distinct intestinal segments.

553 Gastrointestinal symptoms including bloating and diarrhea are the most prevalent
554 side effects of metformin treatment and these symptoms are often experienced in the first
555 few weeks following treatment initiation [50]. It is also well-established that defects in
556 intestinal fructose metabolism can cause significant GI disturbances [51-54]. It is
557 interesting to speculate that the ability of metformin to impair fructose absorption may
558 contribute to its unwanted gastrointestinal effects. Future studies may include
559 investigation into how metformin alters intestinal epithelial absorptive function and
560 substrate transport.

561 Most studies investigating metformin's mechanism of action focus on specific
562 putative targets include Complex 1, AMPK, mitochondrial glycerophosphate
563 dehydrogenase, PEN2, and others [14; 40; 49; 55; 56]. Unexpectedly, our proteomics
564 data conducted on metformin treated intestinal tissue suggests that metformin produces
565 broad-based reductions in the levels of many metabolic enzymes including key enzymes
566 in glycolytic, gluconeogenic, and fructolytic pathways. These results are consistent with
567 our conclusions regarding metformin's multiple metabolic effects derived from isotope
568 tracing data that fructose metabolism, glucose production, and other aspects of intestinal
569 carbohydrate metabolism are all significantly impacted by metformin treatment. This novel
570 finding extends our knowledge of metformin's potential mechanistic effects and points to
571 novel mechanisms of action.

572 Broad-based effects of metformin on the levels of components of the mitochondrial
573 electron transport chain are also indicated by the proteomics data analysis. Metformin is
574 known to regulate mitochondrial function by inhibiting Complex I of the mitochondrial
575 electron transport chain [40]. However, the physiological relevance of this mechanism is
576 debated as this mechanism requires high concentrations of metformin (~ 150 μM) within

577 the mitochondrial matrix [32]. At the therapeutically relevant doses that we used in this
578 study, we observed that metformin reduced citrate levels and increased malate levels in
579 the portal circulation (Figure 4G and H). This suggests inhibition of malate dehydrogenase
580 and Complex I of the electron transport chain as malate dehydrogenase activity is coupled
581 to Complex I activity. However, as the proteomics analysis indicated that the expression
582 levels of many Complex I subunits including multiple Ndufa, Ndufb and Ndufs subunits
583 were significantly down-regulated by metformin treatment (Figure 6A), we cannot
584 determine whether metformin's apparent effect to inhibit Complex I activity might be
585 mediated by direct inhibition or through metformin's more general effect to reduce levels
586 of Complex I components.

587 AMPK activation is often invoked as a key mechanism mediating metformin action
588 [7; 36]. Although, recent studies suggest metformin relies on both AMPK-dependent and
589 AMPK-independent mechanisms to mediate its beneficial effects [9]. We also observed
590 that the intestinal AMPK signaling was impacted by metformin treatment (Figure 6C and
591 D). Metformin increased phosphorylation of AMPK at Thr172 potentially consistent with
592 increased AMP/ATP ratio (Figure 6E and F). Again, because of the broad-based effects
593 of metformin on metabolic and mitochondrial protein levels, we cannot readily define the
594 mechanism by which metformin treatment leads to AMPK activation. Neither could we
595 determine whether AMPK signaling participates in metformin's effects to reduce intestinal
596 fructose metabolism and glucose production.

597 This study supports our recent work indicating that the intestine is a major source
598 of circulating TCA cycle intermediates [31], and that measurement of fructose-derived
599 label in portal and possibly peripheral circulating blood TCA cycle metabolites may
600 provide a useful index of intestinal metabolic function. In the future this approach may be
601 useful for assessing intestinal metabolic function in large-scale human studies and has
602 the potential to open new avenues for investigating intestinal metabolic function in a wide
603 range of scenarios. In this study, we used this approach to demonstrate that the intestine
604 is a target for therapeutic doses of metformin and short-term metformin treatment impacts
605 intestinal glucose and fructose metabolism. Moreover, proteomics analysis suggests that
606 metformin reduces the intestinal levels of a broad array of metabolic enzymes and
607 transporters involved in sugar metabolism. Additional work will be required to define

608 mechanisms by which metformin reduces the levels metabolic enzymes and impacts key
609 metabolic pathways within the intestine to enhance glucose homeostasis.
610
611
612 **Author Contributions:**
613 **MAH, WT, SAH, AS and IA** designed, performed, and interpreted the mouse
614 experiments. **GZ, WT, MAH, and SAH** designed, performed, and interpreted
615 metabolomics analysis. **PAG, MAH, IA, and WT** designed, performed, and interpreted
616 proteomics analysis. **MAH** conceived of, designed, and supervised the experimental plan,
617 and interpreted experiments. **WT** and **MAH** wrote the manuscript. All authors edited the
618 manuscript.
619
620 **Acknowledgements:**
621 This work was supported by NIH grant 5R01 DK121710 (MAH). Metabolomics support
622 was provided by the North Carolina Diabetes Research Center (NCDRC) (P30
623 DK124723).
624
625 **Figure Legends:**
626 **Figure 1. Short-term metformin treatment improves glucose tolerance without**
627 **reducing body weight and fasting glycemia levels.**
628 (A) Body weight before and after metformin versus water treatment. (B) Fasting
629 glycemia levels after 2 weeks of treatment. (C - D) Intraperitoneal glucose tolerance test
630 after 2 weeks of treatment. Data represent means ± SEM. n=9 per group * $p<0.05$; **
631 $p<0.01$; *** $p<0.001$. Analysis performed via paired student-t test.
632
633 **Figure 2. Short-term metformin treatment is sufficient to decrease fructose**
634 **catabolism in the intestinal tissue and fructose delivery to the liver.**
635 (A) Diagram showing the fructose catabolism pathways within enterocytes. (B)
636 Relative quantity of fructose 1-phosphate, and enrichment of (C) glyceraldehyde 3-
637 phosphate, and (D) glycerate in the intestinal tissue 30 minutes after fructose gavage in
638 mice treated with water versus metformin for 2 weeks. (E) Absolute fructose levels

639 measured in the portal blood. (F) Relative quantification of fructose 1-phosphate and (G)
640 glyceraldehyde 3-phosphate in the liver tissue after fructose gavage. 0.1 nmol M6-
641 Fructose 6-phosphate and 4 nmol M2-fructose were used as internal standard for the
642 measurement of fructose 1-phosphate and fructose respectively. Norvaline was used as
643 the internal standard for the measurement of glyceraldehyde 3-phosphate, and glycerate.
644 Data represent means ± SEM. * $p<0.05$; ** $p<0.01$; *** $p<0.001$. Analysis performed via
645 paired student-t test.
646
647 **Figure 3. Short-term metformin treatment reduces glucose production from**
648 **fructose in intestinal tissue.**
649 (A) Relative glucose levels and (B) the enrichment of glucose with labeled fructose tracer
650 in intestinal tissue. (C) Relative circulating glucose and (D) enrichment of glucose
651 measured in tail vein plasma. The levels of glucose with (E) any, (F) three, and (G) no
652 carbons derived from fructose in intestinal tissue. 2 nmol 2-Deoxu-D-glucose (2DG) was
653 used as internal standard for the measurement of glucose. Data represent means ± SEM.
654 * $p<0.05$; ** $p<0.01$; *** $p<0.001$. Analysis performed via paired student-t test.
655
656 **Figure 4. Short-term metformin treatment reduces production of intestinal TCA**
657 **cycle intermediates from fructose.**
658 The enrichment of (A) succinate, (B) malate, and (C) citrate in intestinal tissue 30 minutes
659 after fructose gavage in mice treated with water versus metformin for 2 weeks. The
660 enrichment of (D) succinate, (E) malate, and (F) citrate in the portal plasma after fructose
661 gavage. Relative quantification of TCA cycle metabolites in the (G) intestinal tissue, and
662 (H) portal circulation. Norvaline was used as the internal standard for these
663 measurements. Data represent means ± SEM. * $p<0.05$; ** $p<0.01$; *** $p<0.001$. Analysis
664 performed via paired student-t test.
665
666 **Figure 5. Proteomics demonstrates down-regulation of proteins involved in**
667 **carbohydrate metabolism in intestinal tissue.**
668 (A) Principal component analysis of quantitative proteomics data generated from the
669 intestinal tissue samples of mice treated with water versus metformin. (B) Volcano plot

670 and (C) K-means clustering of differentially abundant proteins in the intestinal tissue
671 samples from water versus metformin groups.
672
673
674
675 (D) Pathway analysis using proteins that are significantly down-regulated in the intestinal
676 tissue samples of metformin versus water group. (E) Significantly altered protein levels in
677 the gluconeogenesis pathway as well as key hexose transporters and fructolytic
678 enzymes. Analysis performed in R using data generated from Proteome Discoverer.
679
680 **Figure 6. Short-term metformin treatment impacts mitochondrial components and**
681 **activates AMPK signaling.**
682 (A) Metformin reduces protein levels of components of the electron transport chain in
683 intestinal tissue. (B) Principal component analysis using proteins annotated in the AMPK
684 signaling pathway (KEGG: mmu04152). (C-D) Intestinal protein abundance in AMPK
685 signaling pathway in water versus metformin group. (E-F) Western blot and quantification
686 of the expression levels of AMPKα and phospho-AMPKα T172. Analysis within panel A
687 and B was performed with R using data generated from Proteome Discoverer. Data in
688 panel F represent as means ± SEM and paired student-t test was used for statistical
689 analysis. * $p<0.05$; ** $p<0.01$; *** $p<0.001$.
690

691 **Reference**

692 [1] Sanchez-Rangel, E., Inzucchi, S.E., 2017. Metformin: clinical use in type 2 diabetes.
693 Diabetologia 60(9):1586-1593.
694 [2] Yerevanian, A., Soukas, A.A., 2019. Metformin: Mechanisms in Human Obesity and
695 Weight Loss. Curr Obes Rep 8(2):156-164.
696 [3] Lin, H.Z., Yang, S.Q., Chuckaree, C., Kuhajda, F., Ronnet, G., Diehl, A.M., 2000.
697 Metformin reverses fatty liver disease in obese, leptin-deficient mice. Nat Med 6(9):998-1003.
698 [4] Farr, S.A., Roesler, E., Niehoff, M.L., Roby, D.A., McKee, A., Morley, J.E., 2019.
699 Metformin Improves Learning and Memory in the SAMP8 Mouse Model of Alzheimer's
700 Disease. J Alzheimers Dis 68(4):1699-1710.
701 [5] Cerezo, M., Tichet, M., Abbe, P., Ohanna, M., Lehraiki, A., Rouaud, F., et al., 2013.
702 Metformin blocks melanoma invasion and metastasis development in AMPK/p53-dependent
703 manner. Mol Cancer Ther 12(8):1605-1615.
704 [6] Linnard-Palmer, L., 2012. The use of simulation for pediatric oncology nursing safety
705 principles: ensuring competent practice through the use of a mnemonic, chemotherapy road
706 maps and case-based learning. J Pediatr Nurs 27(3):283-286.
707 [7] Hundal, R.S., Krssak, M., Dufour, S., Laurent, D., Lebon, V., Chandramouli, V., et al.,
708 2000. Mechanism by which metformin reduces glucose production in type 2 diabetes. Diabetes
709 49(12):2063-2069.
710 [8] LaMoia, T.E., Shulman, G.I., 2021. Cellular and Molecular Mechanisms of Metformin
711 Action. Endocr Rev 42(1):77-96.
712 [9] Rena, G., Hardie, D.G., Pearson, E.R., 2017. The mechanisms of action of metformin.
713 Diabetologia 60(9):1577-1585.
714 [10] Foretz, M., Guigas, B., Bertrand, L., Pollak, M., Viollet, B., 2014. Metformin: from
715 mechanisms of action to therapies. Cell Metab 20(6):953-966.
716 [11] Tanja, J.J., Langlass, T.M., 1995. Metformin: a biguanide. Diabetes Educ 21(6):509-510,
717 513-504.
718 [12] Zhang, Q., Hu, N., 2020. Effects of Metformin on the Gut Microbiota in Obesity and
719 Type 2 Diabetes Mellitus. Diabetes Metab Syndr Obes 13:5003-5014.
720 [13] Tobar, N., Rocha, G.Z., Santos, A., Guadagnini, D., Assalin, H.B., Camargo, J.A., et al.,
721 2023. Metformin acts in the gut and induces gut-liver crosstalk. Proc Natl Acad Sci U S A
722 120(4):e2211933120.
723 [14] Ma, T., Tian, X., Zhang, B., Li, M., Wang, Y., Yang, C., et al., 2022. Low-dose metformin
724 targets the lysosomal AMPK pathway through PEN2. Nature 603(7899):159-165.
725 [15] Yılmaz, S., Ozhan, M., Sager, S., Yörük Atik, D., Halac, M., Sönmezoğlu, K., 2011.
726 Metformin-Induced Intense Bowel Uptake Observed on Restaging FDG PET/CT Study in a
727 Patient with Gastric Lymphoma. Mol Imaging Radionucl Ther 20(3):114-116.
728 [16] Massollo, M., Marini, C., Brignone, M., Emionite, L., Salani, B., Riondato, M., et al., 2013.
729 Metformin temporal and localized effects on gut glucose metabolism assessed using 18F-FDG
730 PET in mice. J Nucl Med 54(2):259-266.
731 [17] Jang, C., Hui, S., Lu, W., Cowan, A.J., Morscher, R.J., Lee, G., et al., 2018. The Small
732 Intestine Converts Dietary Fructose into Glucose and Organic Acids. Cell Metab 27(2):351-
733 361.e353.

[18] Bismut, H., Hers, H.G., Van Schaftingen, E., 1993. Conversion of fructose to glucose in the rabbit small intestine. A reappraisal of the direct pathway. Eur J Biochem 213(2):721-726.
[19] Bu, P., Chen, K.Y., Xiang, K., Johnson, C., Crown, S.B., Rakhilin, N., et al., 2018. Aldolase B-Mediated Fructose Metabolism Drives Metabolic Reprogramming of Colon Cancer Liver Metastasis. Cell Metab 27(6):1249-1262.e1244.
[20] Fernandez, C.A., Des Rosiers, C., Previs, S.F., David, F., Brunengraber, H., 1996. Correction of 13C mass isotopomer distributions for natural stable isotope abundance. J Mass Spectrom 31(3):255-262.
[21] Zhang, G.F., Jensen, M.V., Gray, S.M., El, K., Wang, Y., Lu, D., et al., 2020. Reductive TCA cycle metabolism fuels glutamine- and glucose-stimulated insulin secretion. Cell Metab.
[22] Lyons, S.P., Wilson, R.J., Muoio, D.M., Grimsrud, P.A., 2022. Proteomics and phosphoproteomics datasets of a muscle-specific STIM1 loss-of-function mouse model. Data Brief 42:108051.
[23] Deutsch, E.W., Csordas, A., Sun, Z., Jarnuczak, A., Perez-Riverol, Y., Ternent, T., et al., 2017. The ProteomeXchange consortium in 2017: supporting the cultural change in proteomics public data deposition. Nucleic Acids Res 45(D1):D1100-d1106.
[24] Okuda, S., Watanabe, Y., Moriya, Y., Kawano, S., Yamamoto, T., Matsumoto, M., et al., 2017. jPOSTrepo: an international standard data repository for proteomes. Nucleic Acids Res 45(D1):D1107-d1111.
[25] Love, M.I., Huber, W., Anders, S., 2014. Moderated estimation of fold change and dispersion for RNA-seq data with DESeq2. Genome Biol 15(12):550.
[26] Ritchie, M.E., Phipson, B., Wu, D., Hu, Y., Law, C.W., Shi, W., et al., 2015. limma powers differential expression analyses for RNA-sequencing and microarray studies. Nucleic Acids Res 43(7):e47.
[27] Coll, A.P., Chen, M., Taskar, P., Rimmington, D., Patel, S., Tadross, J.A., et al., 2020. GDF15 mediates the effects of metformin on body weight and energy balance. Nature 578(7795):444-448.
[28] Jensterle Sever, M., Kocjan, T., Pfeifer, M., Kravos, N.A., Janez, A., 2014. Short-term combined treatment with liraglutide and metformin leads to significant weight loss in obese women with polycystic ovary syndrome and previous poor response to metformin. Eur J Endocrinol 170(3):451-459.
[29] Liu, L., Li, T., Liao, Y., Wang, Y., Gao, Y., Hu, H., et al., 2020. Triose Kinase Controls the Lipogenic Potential of Fructose and Dietary Tolerance. Cell Metab 32(4):605-618.e607.
[30] Andres-Hernando, A., Orlicky, D.J., Kuwabara, M., Ishimoto, T., Nakagawa, T., Johnson, R.J., et al., 2020. Deletion of Fructokinase in the Liver or in the Intestine Reveals Differential Effects on Sugar-Induced Metabolic Dysfunction. Cell Metab 32(1):117-127.e113.
[31] Tong, W., Hannou, S.A., Wang, Y., Astapova, I., Sargsyan, A., Monn, R., et al., 2022. The intestine is a major contributor to circulating succinate in mice. Faseb j 36(10):e22546.
[32] Owen, M.R., Doran, E., Halestrap, A.P., 2000. Evidence that metformin exerts its anti-diabetic effects through inhibition of complex 1 of the mitochondrial respiratory chain. Biochem J 348 Pt 3(Pt 3):607-614.

775 [33] Lee, P., Leong, W., Tan, T., Lim, M., Han, W., Radda, G.K., 2013. In vivo hyperpolarized
776 carbon-13 magnetic resonance spectroscopy reveals increased pyruvate carboxylase flux in an
777 insulin-resistant mouse model. Hepatology 57(2):515-524.
778 [34] Wang, Q., Yu, L., Yu, C.A., 2010. Cross-talk between mitochondrial malate
779 dehydrogenase and the cytochrome bc1 complex. J Biol Chem 285(14):10408-10414.
780 [35] Ovádi, J., Huang, Y., Spivey, H.O., 1994. Binding of malate dehydrogenase and NADH
781 channelling to complex I. J Mol Recognit 7(4):265-272.
782 [36] Wang, Y., An, H., Liu, T., Qin, C., Sesaki, H., Guo, S., et al., 2019. Metformin Improves
783 Mitochondrial Respiratory Activity through Activation of AMPK. Cell Rep 29(6):1511-
784 1523.e1515.
785 [37] Yang, M., Darwish, T., Larraufie, P., Rimmington, D., Cimino, I., Goldspink, D.A., et al.,
786 2021. Inhibition of mitochondrial function by metformin increases glucose uptake, glycolysis
787 and GDF-15 release from intestinal cells. Sci Rep 11(1):2529.
788 [38] Vial, G., Detaille, D., Guigas, B., 2019. Role of Mitochondria in the Mechanism(s) of
789 Action of Metformin. Front Endocrinol (Lausanne) 10:294.
790 [39] Soberanes, S., Misharin, A.V., Jairaman, A., Morales-Nebreda, L., McQuattie-Pimentel,
791 A.C., Cho, T., et al., 2019. Metformin Targets Mitochondrial Electron Transport to Reduce Air-
792 Pollution-Induced Thrombosis. Cell Metab 29(2):335-347.e335.
793 [40] Wheaton, W.W., Weinberg, S.E., Hamanaka, R.B., Soberanes, S., Sullivan, L.B., Anso, E.,
794 et al., 2014. Metformin inhibits mitochondrial complex I of cancer cells to reduce tumorigenesis.
795 Elife 3:e02242.
796 [41] Ling, S., Shan, Q., Liu, P., Feng, T., Zhang, X., Xiang, P., et al., 2017. Metformin
797 ameliorates arsenic trioxide hepatotoxicity via inhibiting mitochondrial complex I. Cell Death
798 Dis 8(11):e3159.
799 [42] Buse, J.B., DeFronzo, R.A., Rosenstock, J., Kim, T., Burns, C., Skare, S., et al., 2016. The
800 Primary Glucose-Lowering Effect of Metformin Resides in the Gut, Not the Circulation: Results
801 From Short-term Pharmacokinetic and 12-Week Dose-Ranging Studies. Diabetes Care 39(2):198-
802 205.
803 [43] Sum, C.F., Webster, J.M., Johnson, A.B., Catalano, C., Cooper, B.G., Taylor, R., 1992. The
804 effect of intravenous metformin on glucose metabolism during hyperglycaemia in type 2
805 diabetes. Diabet Med 9(1):61-65.
806 [44] Gontier, E., Fourme, E., Wartski, M., Blondet, C., Bonardel, G., Le Stanc, E., et al., 2008.
807 High and typical 18F-FDG bowel uptake in patients treated with metformin. Eur J Nucl Med
808 Mol Imaging 35(1):95-99.
809 [45] Herman, M.A., Birnbaum, M.J., 2021. Molecular aspects of fructose metabolism and
810 metabolic disease. Cell Metab 33(12):2329-2354.
811 [46] Khan, T.A., Sievenpiper, J.L., 2016. Controversies about sugars: results from systematic
812 reviews and meta-analyses on obesity, cardiometabolic disease and diabetes. Eur J Nutr
813 55(Suppl 2):25-43.
814 [47] Ma, J., McKeown, N.M., Hwang, S.J., Hoffmann, U., Jacques, P.F., Fox, C.S., 2016. Sugar-
815 Sweetened Beverage Consumption Is Associated With Change of Visceral Adipose Tissue Over
816 6 Years of Follow-Up. Circulation 133(4):370-377.

817 [48] Toop, C.R., Gentili, S., 2016. Fructose Beverage Consumption Induces a Metabolic
818 Syndrome Phenotype in the Rat: A Systematic Review and Meta-Analysis. Nutrients 8(9).
819 [49] Spruss, A., Kanuri, G., Stahl, C., Bischoff, S.C., Bergheim, I., 2012. Metformin protects
820 against the development of fructose-induced steatosis in mice: role of the intestinal barrier
821 function. Lab Invest 92(7):1020-1032.
822 [50] Subramaniam, K., Joseph, M.P., Babu, L.A., 2021. A Common Drug Causing a Common
823 Side Effect at an Uncommon Time: Metformin-Induced Chronic Diarrhea and Weight Loss
824 After Years of Treatment. Clin Diabetes 39(2):237-240.
825 [51] Choi, Y.K., Johlin, F.C., Jr., Summers, R.W., Jackson, M., Rao, S.S., 2003. Fructose
826 intolerance: an under-recognized problem. Am J Gastroenterol 98(6):1348-1353.
827 [52] Barone, S., Fussell, S.L., Singh, A.K., Lucas, F., Xu, J., Kim, C., et al., 2009. Slc2a5 (Glut5)
828 is essential for the absorption of fructose in the intestine and generation of fructose-induced
829 hypertension. J Biol Chem 284(8):5056-5066.
830 [53] Patel, C., Douard, V., Yu, S., Gao, N., Ferraris, R.P., 2015. Transport, metabolism, and
831 endosomal trafficking-dependent regulation of intestinal fructose absorption. Faseb j 29(9):4046-
832 4058.
833 [54] Kim, M., Astapova, II, Flier, S.N., Hannou, S.A., Doridot, L., Sargsyan, A., et al., 2017.
834 Intestinal, but not hepatic, ChREBP is required for fructose tolerance. JCI Insight 2(24).
835 [55] Cao, J., Meng, S., Chang, E., Beckwith-Fickas, K., Xiong, L., Cole, R.N., et al., 2014. Low
836 concentrations of metformin suppress glucose production in hepatocytes through AMP-
837 activated protein kinase (AMPK). J Biol Chem 289(30):20435-20446.
838 [56] Thakur, S., Daley, B., Gaskins, K., Vasko, V.V., Boufraqech, M., Patel, D., et al., 2018.
839 Metformin Targets Mitochondrial Glycerophosphate Dehydrogenase to Control Rate of
840 Oxidative Phosphorylation and Growth of Thyroid Cancer In Vitro and In Vivo. Clin Cancer
841 Res 24(16):4030-4043.
842

Figure1

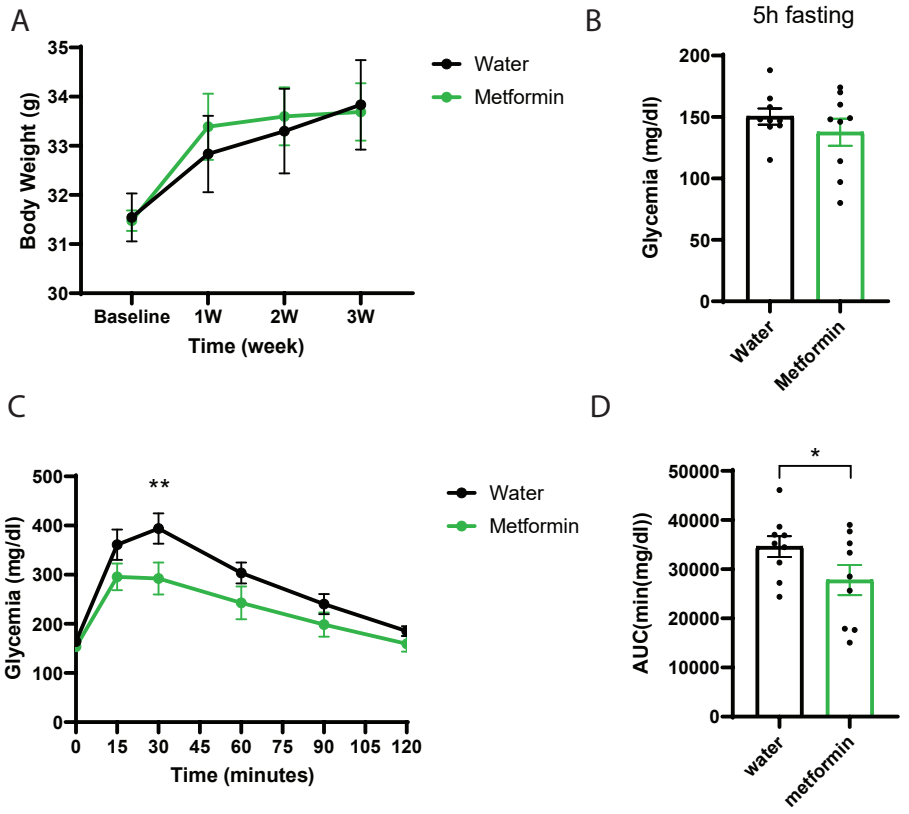
A
Body Weight (g)
35
34
33
32
31
30
Baseline
1W
2W
3W
Time (week)
Water
Metformin
B
5h fasting
Glycemia (mg/dl)
200
150
100
50
0
Water
Metformin
C
Glycemia (mg/dl)
500
400
300
200
100
0
**
0
15
30
45
60
75
90
105
120
Time (minutes)
Water
Metformin
D
AUC(min(mg/dl))
50000
40000
30000
20000
10000
0
*
water
metformin

Figure 2

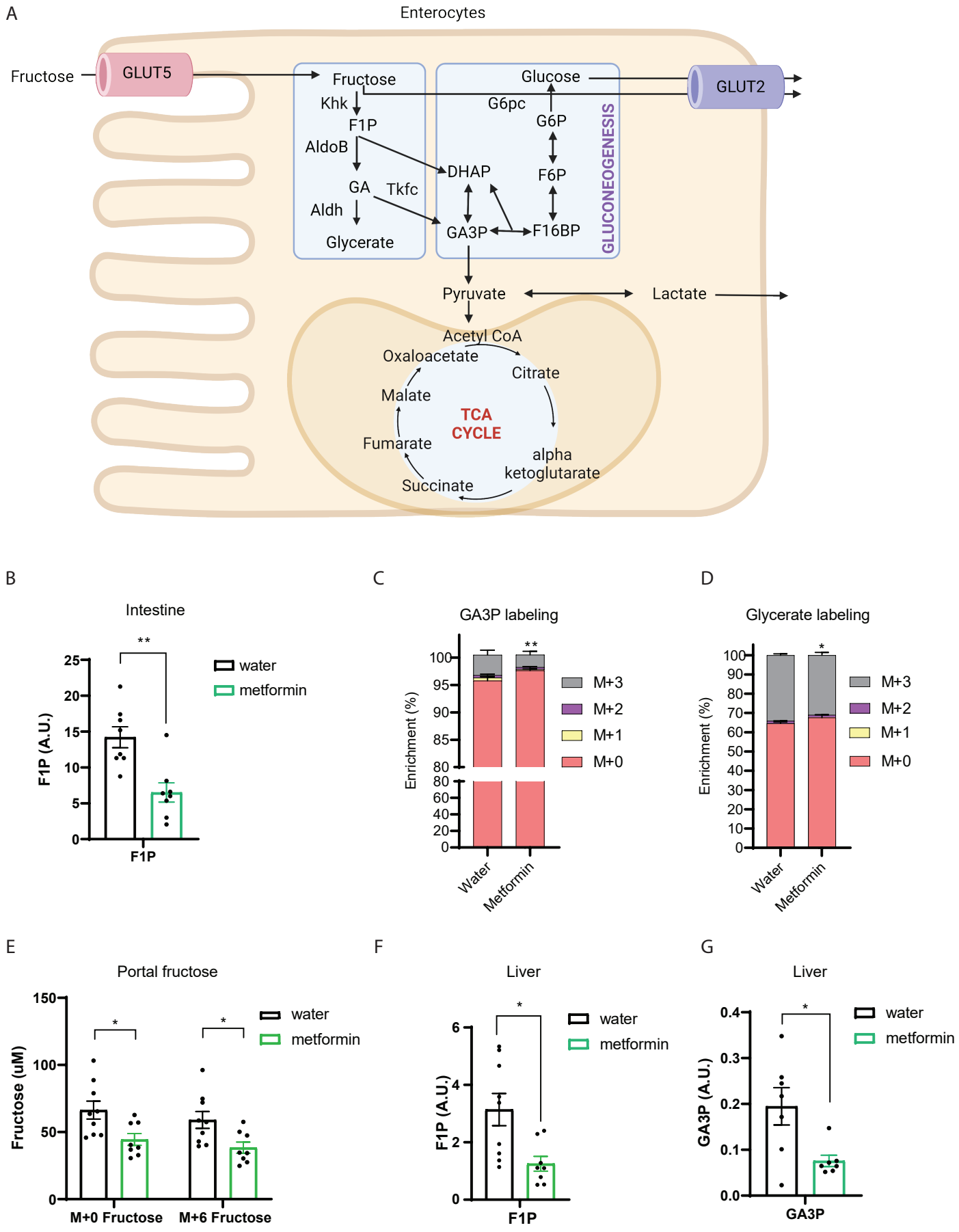
A
Enterocytes
Fructose
GLUT5
Fructose
Khk
F1P
AldoB
GA
Tkfc
Aldh
Glycerate
Glucose
G6pc
G6P
F6P
DHAP
GA3P
F16BP
GLUCONEOGENESIS
GLUT2
Pyruvate
Lactate
Acetyl CoA
Oxaloacetate
Citrate
Malate
TCA CYCLE
Fumarate
alpha ketoglutarate
Succinate
B
Intestine
F1P (A.U.)
F1P
water
metformin
C
GA3P labeling
Enrichment (%)
M+3
M+2
M+1
M+0
Water
Metformin
D
Glycerate labeling
Enrichment (%)
M+3
M+2
M+1
M+0
Water
Metformin
E
Portal fructose
Fructose (uM)
M+0 Fructose
M+6 Fructose
water
metformin
F
Liver
F1P (A.U.)
F1P
water
metformin
G
Liver
GA3P (A.U.)
GA3P
water
metformin

Figure 3

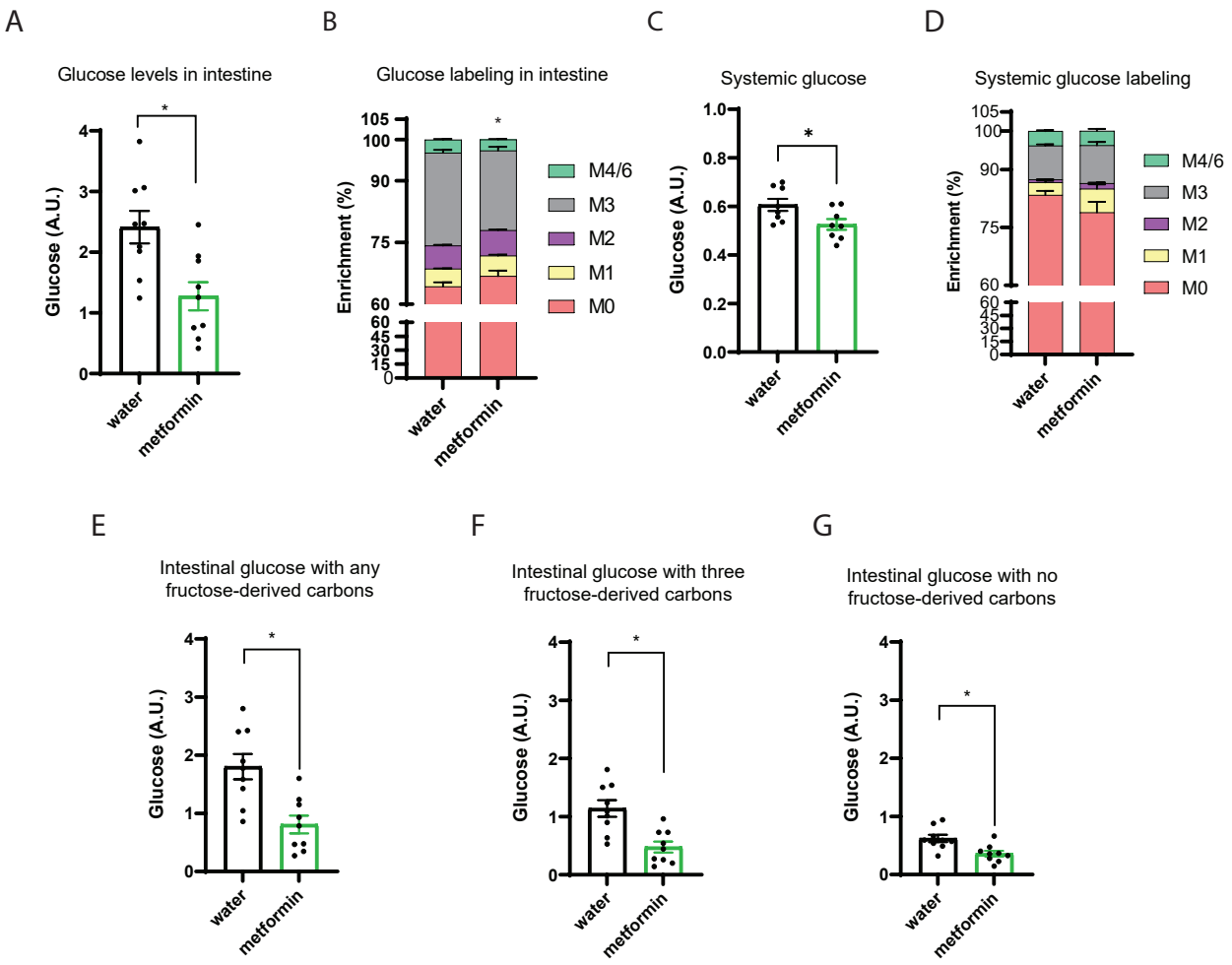
A
Glucose levels in intestine
Glucose (A.U.)
water
metformin
B
Glucose labeling in intestine
Enrichment (%)
M4/6
M3
M2
M1
M0
C
Systemic glucose
D
Systemic glucose labeling
E
Intestinal glucose with any fructose-derived carbons
F
Intestinal glucose with three fructose-derived carbons
G
Intestinal glucose with no fructose-derived carbons

Figure 4

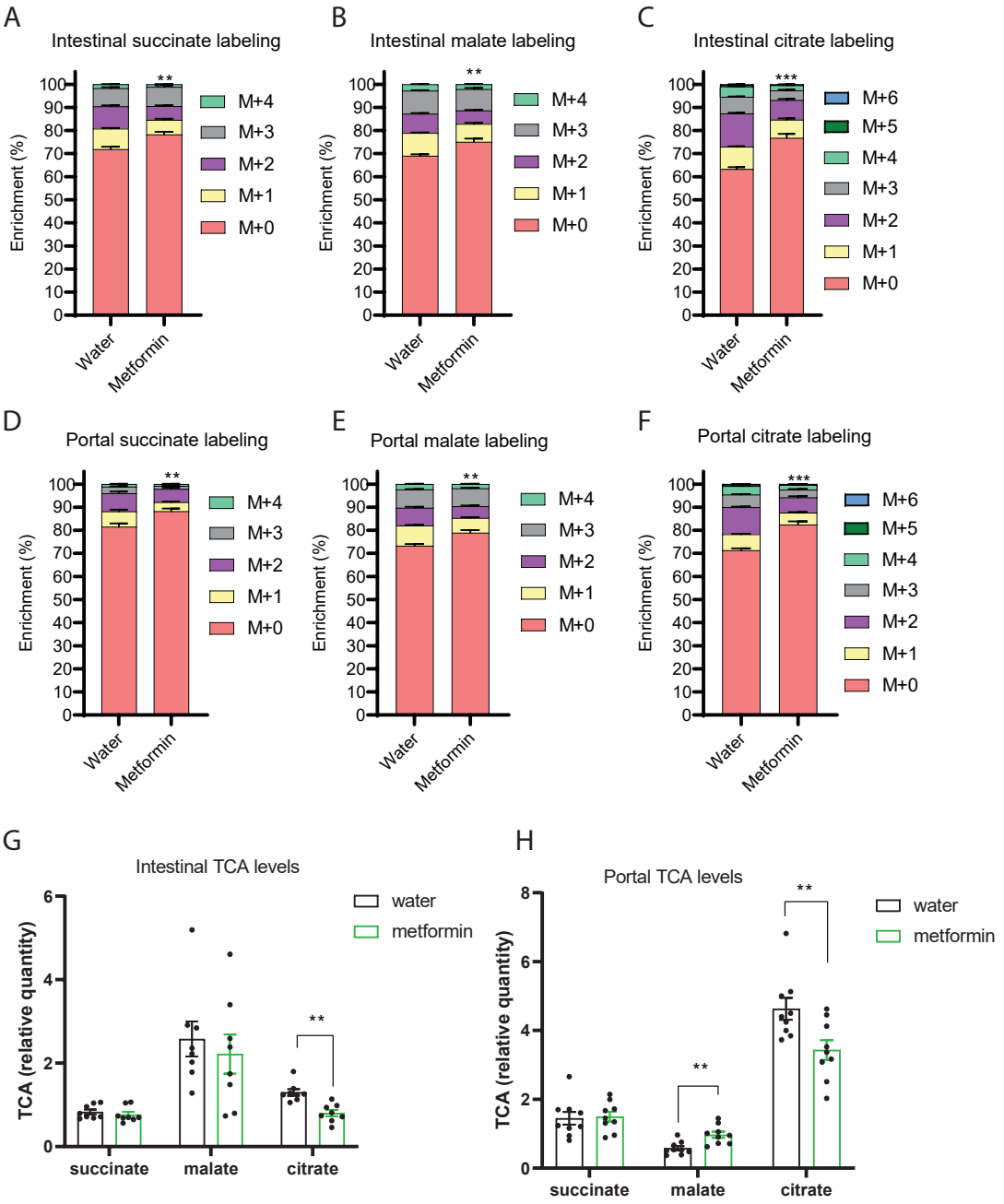
A
Intestinal succinate labeling
B
Intestinal malate labeling
C
Intestinal citrate labeling
D
Portal succinate labeling
E
Portal malate labeling
F
Portal citrate labeling
Enrichment (%)
Water
Metformin
M+6
M+5
M+4
M+3
M+2
M+1
M+0
G
Intestinal TCA levels
H
Portal TCA levels
TCA (relative quantity)
water
metformin
succinate
malate
citrate

Figure 5

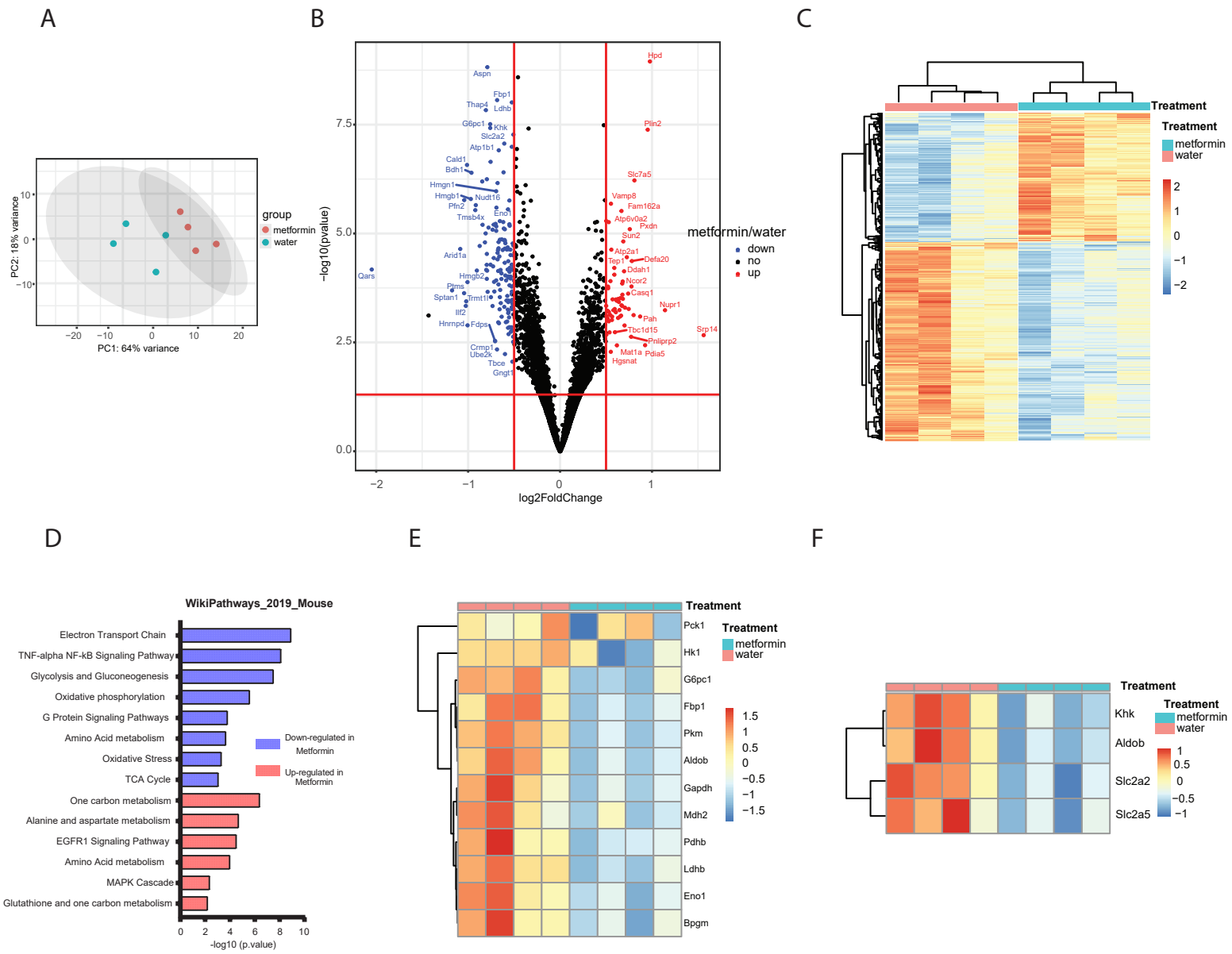
A
PC2: 18% variance
PC1: 64% variance
group
metformin
water
B
−log10(pvalue)
log2FoldChange
metformin/water
down
no
up
C
Treatment
metformin
water
D
WikiPathways_2019_Mouse
Electron Transport Chain
TNF-alpha NF-kB Signaling Pathway
Glycolysis and Gluconeogenesis
Oxidative phosphorylation
G Protein Signaling Pathways
Amino Acid metabolism
Oxidative Stress
TCA Cycle
One carbon metabolism
Alanine and aspartate metabolism
EGFR1 Signaling Pathway
Amino Acid metabolism
MAPK Cascade
Glutathione and one carbon metabolism
Down-regulated in Metformin
Up-regulated in Metformin
-log10 (p.value)
E
Pck1
Hk1
G6pc1
Fbp1
Pkm
Aldob
Gapdh
Mdh2
Pdhb
Ldhb
Eno1
Bpgm
F
Khk
Aldob
Slc2a2
Slc2a5

Figure 6

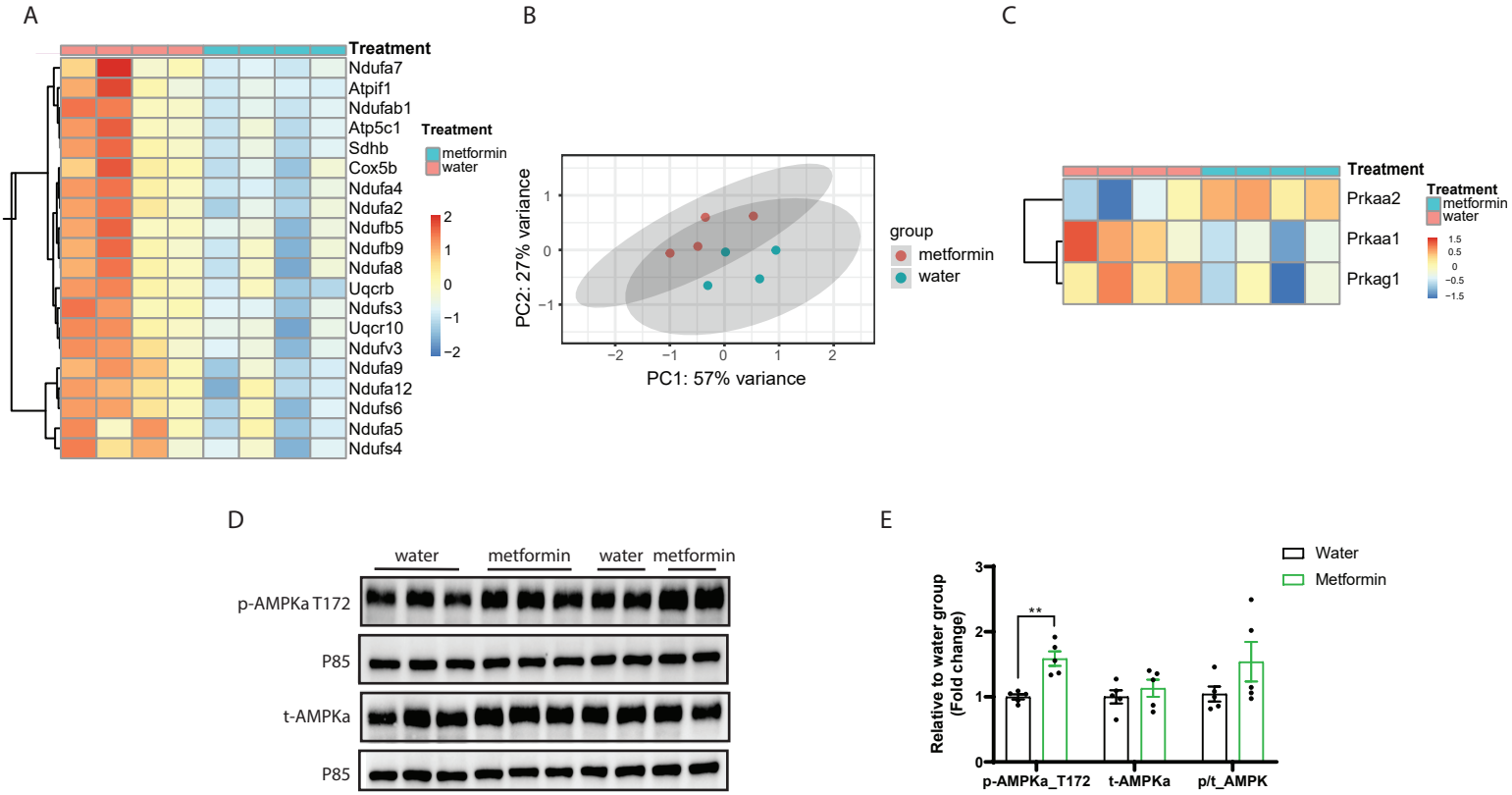
A
Treatment
Ndufa7
Atpif1
Ndufab1
Atp5c1
Sdhb
Cox5b
Ndufa4
Ndufa2
Ndufb5
Ndufb9
Ndufa8
Uqcrb
Ndufs3
Uqcr10
Ndufv3
Ndufa9
Ndufa12
Ndufs6
Ndufa5
Ndufs4
Treatment
metformin
water
2
1
0
−1
−2
B
PC2: 27% variance
PC1: 57% variance
group
metformin
water
C
Treatment
Prkaa2
Prkaa1
Prkag1
Treatment
metformin
water
1.5
0.5
0
−0.5
−1.5
D
water
metformin
water
metformin
p-AMPKa T172
P85
t-AMPKa
P85
E
Water
Metformin
Relative to water group (Fold change)
**
p-AMPKa_T172
t-AMPKa
p/t_AMPK